ResearchGate

See discussions, stats, and author profiles for this publication at: https://www.researchgate.net/publication/224130713

A Vision-Based Self-Tuning Fuzzy Controller for Fillet Weld Seam Tracking

Article *in* IEEE/ASME Transactions on Mechatronics · July 2011

DOI: 10.1109/TMECH.2010.2045766 · Source: IEEE Xplore

CITATIONS
70

READS
124

3 authors:

Zaojun Fang
Chinese Academy of Sciences
24 PUBLICATIONS **228** CITATIONS
SEE PROFILE

De Xu
Chinese Academy of Sciences
163 PUBLICATIONS **1,531** CITATIONS
SEE PROFILE

M. H. Tan
Chinese Academy of Sciences
493 PUBLICATIONS **7,469** CITATIONS
SEE PROFILE

Some of the authors of this publication are also working on these related projects:

ROBOT CONTROLER View project

Smart Robotic Fish View project

All content following this page was uploaded by De Xu on 19 February 2014.

The user has requested enhancement of the downloaded file.

A Vision-Based Self-Tuning Fuzzy Controller for Fillet Weld Seam Tracking

Zaojun Fang, De Xu, *Senior Member, IEEE*, and Min Tan

***Abstract*—In this paper, an intelligent seam-tracking system is developed for fillet weld workpiece. Structured light vision is employed to detect the deviation of the welding torch. Two stripe lines are formed on the surface of the fillet weld workpiece by the structured laser light. Their intercepts are selected as the image feature, which can result in an approximately uncoupled relationship between the image feature and the movement of adjustment mechanism. A two-step feature-extraction method is designed to robustly detect the two lines in image. In order to get a favorable tracking precision in the welding process, a new self-tuning fuzzy controller is designed. Its input and output scaling factors are tuned according to its active working region. Moreover, a supervisory level is introduced into the control system to limit the output pulses in order to guarantee steady and safe tracking. Finally, experiments are well conducted to verify the performance of the proposed system and methods.**

***Index Terms*—Fillet weld, fuzzy controller, image-based visual control, seam tracking, self-tuning, structured light vision.**

I. Introduction

THE LACK of flexibility of existing welding robots cannot satisfy the increasing demand for high weld quality. At present, most of welding robots work in the so-called "teach-by-show" mode. This mode places great demand on the consistent shape and precise position of workpieces. Any deviation of the weld joint from the ideal condition may cause poor-weld quality. Thus, it is very important to develop an intelligent seam-tracking system in order to improve the weld quality.

One distinct feature of intelligent seam-tracking systems is that they can sense the seam information by some kinds of sensors and adjust the torch positions accordingly. Thus, sensors must be adopted. In the last decades, many types of sensors have been developed and used in welding robots, such as acoustic, ultrasonic, through-the-arc, electromagnetic, and inductive sensors [1]–[5]. Recently, vision sensors have received more and more attention due to their high precision and rich information [6]–[10]. Among them, the ones based on structured laser light are largely used in welding process due to the monochromaticity and robustness of laser light. Though many seam-tracking systems have been designed with structured light vision sensors [11]–[13], they cannot be applied to track fillet weld seams directly. One reason is that the image feature should be carefully selected to get an uncoupled relationship between the movement of the cross mechanism and the image feature change. Another reason is that conventional controller, such as PID controller and regular fuzzy controller (RFC) cannot get fine performance in fillet weld seam tracking.

In visual seam-tracking systems, two types of visual control methods can be utilized [14]: namely, position-based visual servoing (PBVS) and image-based visual servoing (IBVS). PBVS is adopted in most of the visual seam-tracking systems, since its control law can be designed easily [12], [13], [15], [16]. In these systems, the weld joint was segmented and recognized in images, and then, 3-D model of the joint was built online for real-time tracking. It is clear that any errors in the camera calibration will lead to the errors in 3-D reconstruction, and subsequently, to tracking errors. However, the merits of IBVS are that it is robust to camera calibration errors and the tracking precision is higher. Xu [11] used IBVS to design a seam-tracking system. The error correction of the welding robot along the seam was based on a properly designed image Jacobian matrix. The problem is that the computation of image Jacobian matrix is time-consuming.

Arc welding is a nonlinear, time-varying, and uncertain process [17]. For such a process, fuzzy controller is a good candidate, since it is not based on the model of the process and can employ some useful regulation rules from the operators. A systematic design procedure for fuzzy controller in servo systems is given in [18]. RFC is not suitable to control welding seam tracking due to its lack of adaption to the time-varying process. To improve the response, some autoadjusting mechanisms need to be introduced. Recently, many self-tuning or self-organizing mechanisms for fuzzy controller have been presented [19]–[24]. In [19], modulated orthogonal membership functions were utilized to reduce the parameters of the rule base, and genetic algorithms were proposed to learn the fuzzy rules. In [20], both the input and output scaling factors were adjusted by a common coefficient, which was regulated by a properly designed rule base. Moreover, a conditional integration was added to the fuzzy controller to diminish the steady-state error. Kwong and Passino [22] proposed three types of self-tuning mechanisms and gave some comparison between them. Langari and Tomizuka [23] presented a self-organizing fuzzy controller in which the shapes of the membership functions of the controller were modified using the hill climbing approach to reflect the

Manuscript received September 27, 2009; revised March 4, 2010; accepted March 6, 2010. Date of publication April 12, 2010; date of current version May 6, 2011. Recommended by Technical Editor S. Fatikow. This work was supported in part by the National High Technology Research and Development Program of China under Grant 2006AA04Z213 and in part by the National Natural Science Foundation of China under Grant 60725309.

The authors are with the Key Laboratory of Complex Systems and Intelligence Science, Institute of Automation, Chinese Academy of Sciences, Beijing 100190, China (e-mail: fzaoj@163.com; sdxude@yahoo.com; tan@compsys.ia.ac.cn).

Color versions of one or more of the figures in this paper are available online at http://ieeexplore.ieee.org.

Digital Object Identifier 10.1109/TMECH.2010.2045766

1083-4435/$26.00 © 2010 IEEE

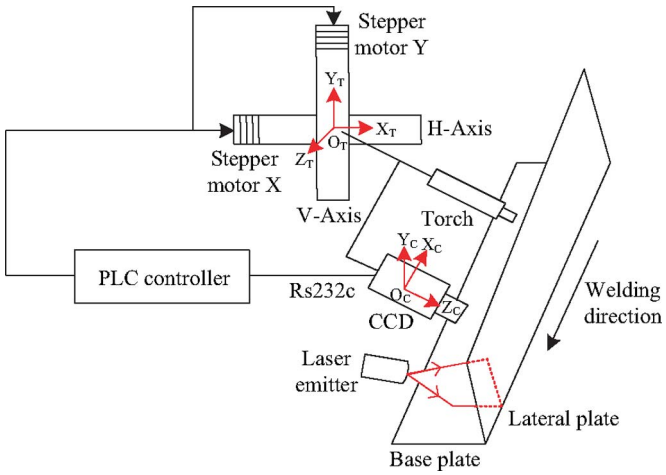

Fig. 1. Block diagram of the seam-tracking system.

new information regarding the behavior of the process. Another self-organizing mechanism was presented in [24]. A reference model was designed and the centers of the output membership functions were moved, based on the deviation of the output of the fuzzy controller from that of the reference model. The self-tuning methods presented earlier have some drawbacks. They complicate the controller structure dramatically, such as the ones based on a special rule base or need some elaborately designed complex algorithms that have high-computational cost, such as the self-organizing methods.

In this paper, an intelligent visual seam-tracking system is designed, which has three distinguish advantages. Firstly, a smart camera is used as the vision sensor and a programmable logic controller (PLC) as the controller. The two components are high reliable and compact. They are easy to be added in the traditional welding systems as accessional components. Secondly, IBVS is adopted as the control method. Reference and feedback image features are defined properly to form a closed loop in the image space. 3-D reconstruction and image Jacobian matrix are not necessary. Thirdly, a new self-tuning fuzzy controller (SFC) is designed, which adjusts its active working region to a best one by autotuning its input and output scaling factors. This new self-tuning mechanism is more efficient and easier to be implemented.

The rest of this paper is organized as follows. Section II describes the system configuration and the vision model. Section III gives the two-step feature-extraction method. The detailed design of the SFC is presented in Section IV. In Section V, experiments and results are provided to verify the proposed system and methods. Finally, this paper is concluded in Section VI.

II. System Description and Modeling

A. System Configuration

The seam-tracking system in this work consists of a cross mechanism, a charge-coupled device (CCD) camera, a laser emitter, a PLC, and welding components, including welding source, welding torch, and wire feeder, etc., as shown in Fig. 1. The cross mechanism has two adjusting axes denoted as H-axis and V-axis that are orthogonal. H-axis is moved in horizontal direction and V-axis in vertical direction. Each axis is driven by a stepper motor. V-axis is mounted on the slider of H-axis. The CCD camera and the torch are fixed on the slider of V-axis via a bracket. The CCD camera is set ahead of the torch by a fixed distance. Its view direction is the same as the direction of the torch. In this way, the deviation of the torch from the welding seam can be directly reflected in image. The CCD camera captures the laser stripe image, computes the image feature and sends it to the PLC. The PLC outputs pulses to the two stepper motors to drive the torch tracking the welding seam. The seam-tracking system is mounted on a vehicle, which is moved on the tracks.

B. Vision Modeling

Two coordinate frames are established, as shown in Fig. 1. The tool frame T is established at the intersection of H-axis and V-axis. Its axes X_T and Y_T are parallel with H-axis and V-axis, respectively. The camera frame C is established at the optical center of the camera. Its Z_C-axis is aligned to the optical line, its X_C-axis and Y_C-axis are the same as those of the image plane. The camera is well adjusted, so that the plane $X_C O_C Y_C$ is approximately parallel with the plane $X_T O_T Z_T$.

Suppose that a point in the frame C is (x_c, y_c, z_c) and the corresponding point in the image is (u, v). From the camera's affine projection model [14], we have

$$\begin{bmatrix} u \\ v \\ 1 \end{bmatrix} = T_1 \begin{bmatrix} x_c \\ y_c \\ z_c \\ 1 \end{bmatrix} = \begin{bmatrix} a_{11} & a_{12} & a_{13} & a_{14} \\ a_{21} & a_{22} & a_{23} & a_{24} \\ 0 & 0 & 0 & 1 \end{bmatrix} \begin{bmatrix} x_c \\ y_c \\ z_c \\ 1 \end{bmatrix} \tag{1}$$

where T_1 is the mapping matrix from the frame C to image coordinates a_{ij}, $(i = 1, 2$ and $j = 1, 2, 3)$ are the gain coefficients, and a_{14} and a_{24} are the offsets.

The transformation from the frame T to the frame C is described as follows:

$$\begin{bmatrix} x_c \\ y_c \\ z_c \\ 1 \end{bmatrix} = T_2 \begin{bmatrix} x_t \\ y_t \\ z_t \\ 1 \end{bmatrix} = \begin{bmatrix} \cos\theta & -\sin\theta & 0 & d_x \\ 0 & 0 & -1 & d_y \\ \sin\theta & \cos\theta & 0 & d_z \\ 0 & 0 & 0 & 1 \end{bmatrix} \begin{bmatrix} x_t \\ y_t \\ z_t \\ 1 \end{bmatrix} \tag{2}$$

where T_2 is the homogeneous transformation matrix from the frame T to the frame C, (x_t, y_t, z_t) are the coordinates of the point in the frame T, (d_x, d_y, d_z) are the displacements from the frame T to the frame C, and θ is the angle between X_C-axis and X_T-axis.

From (1) and (2), the transformation from the point (x_t, y_t, z_t) to its image (u, v) is given by

$$\begin{bmatrix} u \\ v \\ 1 \end{bmatrix} = T_1 T_2 \begin{bmatrix} x_t \\ y_t \\ z_t \\ 1 \end{bmatrix} = \begin{bmatrix} t_{11} & t_{12} & t_{13} & t_{14} \\ t_{21} & t_{21} & t_{23} & t_{24} \\ 0 & 0 & 0 & 1 \end{bmatrix} \begin{bmatrix} x_t \\ y_t \\ z_t \\ 1 \end{bmatrix} \tag{3}$$

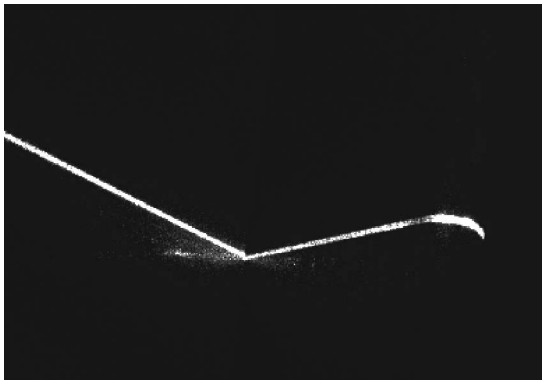

Fig. 2. Laser stripe image.

where

$$\begin{cases} t_{11} = a_{11}\cos\theta + a_{13}\sin\theta \\ t_{12} = -a_{11}\sin\theta + a_{13}\cos\theta \\ t_{13} = -a_{12} \\ t_{14} = a_{11}d_x + a_{12}d_y + a_{13}d_z + a_{14} \\ t_{21} = a_{21}\cos\theta + a_{23}\sin\theta \\ t_{22} = -a_{21}\sin\theta + a_{23}\cos\theta \\ t_{23} = -a_{22} \\ t_{24} = a_{21}d_x + a_{22}d_y + a_{23}d_z + a_{24}. \end{cases}$$

As shown in Fig. 1, the lateral plate surface (LPS) is nearly parallel to Y_T-axis. Therefore, the laser stripe line on the LPS is approximately described in the frame T as follows:

$$\begin{cases} a_1 x + c_1 z + d_1 = 0 \\ ax + by + cz + d = 0 \end{cases} \tag{4}$$

where (a_1, c_1, d_1) and (a, b, c, d) are the parameters of the LPS plane and the laser plane, respectively.

Suppose that two points p_1 and p_2 on the laser stripe on the LPS are (x_1, y_1, z_1) and (x_2, y_2, z_2) in the frame T. From (3), their image points I_1 and I_2 are computed as follows:

$$\begin{bmatrix} u_i \\ v_i \\ 1 \end{bmatrix} = T_1 T_2 \begin{bmatrix} x_i \\ y_i \\ z_i \\ 1 \end{bmatrix} = \begin{bmatrix} t_{11}x_i + t_{12}y_i + t_{13}z_i + t_{14} \\ t_{21}x_i + t_{22}y_i + t_{23}z_i + t_{24} \\ 1 \end{bmatrix} \tag{5}$$

where (u_i, v_i) are the image coordinates of I_i, $i = 1, 2$.

As shown in Fig. 2, the left line in the image is formed from the laser stripe on the LPS. From (5), its slope and intercept are computed as follows:

$$\begin{cases} K_l = \dfrac{t_{21}(x_2 - x_1) + t_{22}(y_2 - y_1) + t_{23}(z_2 - z_1)}{t_{11}(x_2 - x_1) + t_{12}(y_2 - y_1) + t_{13}(z_2 - z_1)} \\ B_l = t_{21}x_1 + t_{22}y_1 + t_{23}z_1 + t_{24} \\ \qquad -K_l(t_{11}x_1 + t_{12}y_1 + t_{13}z_1 + t_{14}) \end{cases} \tag{6}$$

where K_l and B_l are the slope and intercept of the left line in the image, respectively.

The laser plane is stationary in the frame T, even if H-axis and V-axis are adjusted, since the laser emitter and the camera are simultaneously moved with the cross mechanism. Hence, the second equation in (4) is unchanged. Obviously, when only V-axis is adjusted, the LPS plane is kept in the frame T and the first equation in (4) is unchanged. When only H-axis is adjusted by Δx, the LPS plane is translated along X_T-axis, and the first equation in (4) is changed. Equation (4) becomes

$$\begin{cases} a_1(x - \Delta x) + c_1 z + d_1 = 0 \\ ax + by + cz + d = 0. \end{cases} \tag{7}$$

From (7), p_1 and p_2 are transformed to p_1' and p_2' after the movement of H-axis

$$\begin{cases} p_1' = \left(x_1 + \Delta x, y_1 - \dfrac{a}{b}\Delta x, z_1\right) \\ p_2' = \left(x_2 + \Delta x, y_2 - \dfrac{a}{b}\Delta x, z_2\right). \end{cases} \tag{8}$$

From (3) and (8), the image points of p_1' and p_2' denoted as I_1' and I_2' are computed as follows:

$$\begin{bmatrix} u_i' \\ v_i' \\ 1 \end{bmatrix} = \begin{bmatrix} t_{11}(x_i + \Delta x) + t_{12}\left(y_i - \dfrac{a}{b}\Delta x\right) + t_{13}z_i + t_{14} \\ t_{21}(x_i + \Delta x) + t_{22}\left(y_i - \dfrac{a}{b}\Delta x\right) + t_{23}z_i + t_{14} \\ 1 \end{bmatrix} \tag{9}$$

where (u_i', v_i') are the image coordinates of I_i', $i = 1, 2$.

From (9), the slope and intercept of the left line in the image after the movement of H-axis are as follows:

$$\begin{cases} K_l' = \dfrac{t_{21}(x_2 - x_1) + t_{22}(y_2 - y_1) + t_{23}(z_2 - z_1)}{t_{11}(x_2 - x_1) + t_{12}(y_2 - y_1) + t_{13}(z_2 - z_1)} \\ B_l' = B_l + \left[t_{21} - K_l t_{11} + (K_l t_{12} - t_{22})\dfrac{a}{b}\right]\Delta x \end{cases} \tag{10}$$

where K_l' and B_l' are its slope and intercept, respectively.

From (6) and (10), we have

$$\begin{cases} K_l' - K_l = 0 \\ B_l' - B_l = \left[t_{21} - K_l t_{11} + (K_l t_{12} - t_{22})\dfrac{a}{b}\right]\Delta x. \end{cases} \tag{11}$$

It can be seen from (11) that the slope of the left line in image is not changed during the movement of H-axis, while the intercept is changed linearly. However, since the movement of V-axis does not change the LPS plane and the laser plane, neither its slope nor its intercept is changed by the movement of V-axis.

Similarly, the slope of the right line in the image mapped from the laser stripe on the base plate surface (BPS) is not changed by the movement of V-axis, while the intercept is changed linearly and the movement of H-axis does not have effect on them, as shown in the following equation:

$$\begin{cases} K_r' - K_r = 0 \\ B_r' - B_r = \left[t_{21} - K_r t_{11} + (K_r t_{12} - t_{22})\dfrac{a}{b}\right]\Delta y \end{cases} \tag{12}$$

where Δy is the movement of V-axis, K_r and B_r are the slope and intercept of the right line in image before V-axis is moved, and K_r' and B_r' are those after V-axis is moved.

It can be found from (11) and (12) that the control system could be uncoupled if the intercepts of the two stripe lines

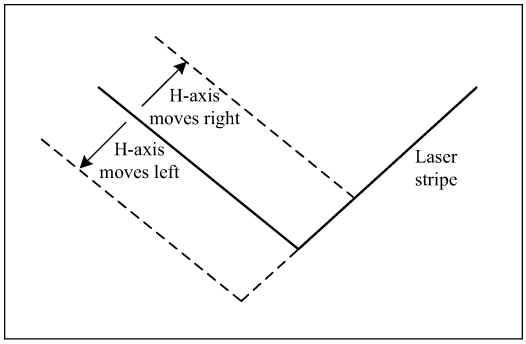

(a)

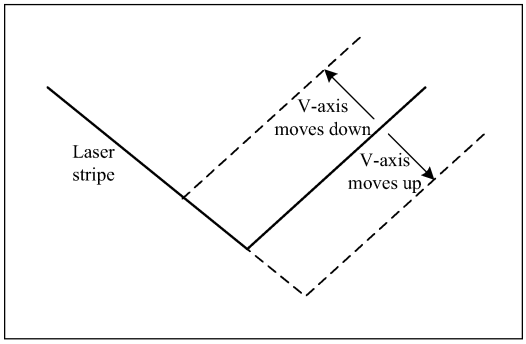

(b)

Fig. 3. Relationship between the movement of two axes and the change of the intercepts of the stripe lines. (a) Left line intercept with the movement of H-axis. (b) Right line intercept with the movement of V-axis.

1	0	0	0	0	0	1
1	1	0	0	0	1	1
1	1	1	0	1	1	1
0	1	1	1	1	1	0
0	0	1	1	1	0	0

(a)

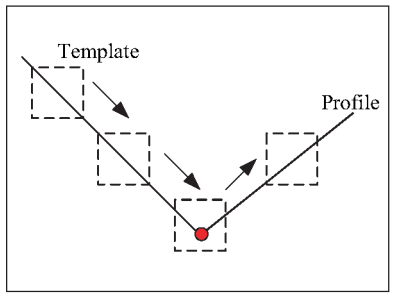

(b)

Fig. 4. Template and the matching process. (a) Template. (b) Template matching process.

were selected as the image feature. The uncoupled relationship between the image feature change and the movement of the cross mechanism is described as follows. The intercept of the left stripe line is proportional to the movement of H-axis, and the intercept of the right stripe line is proportional to the movement of V-axis, as shown in Fig. 3. Therefore, the image-based control method will be very suitable to track the fillet weld seam.

The reference and the feedback image features are defined as follows. The reference image feature is computed using N images at the start stage in the welding process after the torch is manually aligned with the seam. It is kept in the welding process, since only line seam is considered here and the torch orientation is unchangeable with respect to the seam. The feedback image feature is extracted from current image.

III. Image Processing for Fillet Weld Seam

The image processing algorithms for the reference and feedback image features are different. For the reference one, the image processing is composed of two steps. Firstly, the region of interest (ROI) of the image is determined. Then, the feature lines are extracted in the small region defined by the ROI. For the feedback one, only the step of lines extraction is carried out in the ROI.

A. ROI Computation

ROI of the seam image is a small region around the intersection point of the two stripe lines. It is computed by a process named profile following template matching. It is known that conventional template matching process runs in the image from left to right and from top to bottom. Compared with conventional one, the proposed matching method is much more efficient.

Firstly, the profile of the laser stripe is detected. The upper border of the laser stripe is considered as the profile. It is detected by computing the greatest gradient gray value in each column as follows:

$$P_f(j) = \arg\max_k G(k), \quad j = 1, 2, \ldots, w \tag{13}$$

$$G(k) = \sum_{i=k}^{k+4} \alpha_{i-k+1} I(i,j) - \sum_{i=k-5}^{k-1} \alpha_{i-k+6} I(i,j) \tag{14}$$

where $P_f(j)$ is the profile point in jth column, $G(k)$ is the gradient gray value in kth point of jth column, $I(i,j)$ is the gray value of pixel point (i,j), w is the width of the image, and $\alpha_i (i = 1, 2, \ldots, 5)$ are the coefficients of the gradient operator.

If a pixel point is in the profile, it is set to 1. Otherwise, it is set to 0. Thus, the image is binarized. In the binary image, correlation values are calculated along the profile of the laser stripe as follows:

$$R(i,j) = \sum_{x=0}^{L-1} \sum_{y=0}^{K-1} I(x+i, y+j) m(x,y) \tag{15}$$

where $j = 1, 3, 5, \ldots, 2w-1$, $i = P_f(j)$, $R(i,j)$ is the correlation value in pixel point (i,j), $m(x,y)$ is the template, and L and K is the length and width of the template. The template and the matching process are shown in Fig. 4.

Suppose the profile point (i_c, j_c) has the greatest correlation value, then the ROI of the seam image is determined by

$$\begin{cases} [X_{\min}, X_{\max}] = [i_c - \Delta w, i_c + \Delta w] \\ [Y_{\min}, Y_{\max}] = [j_c - \Delta h, j_c + \Delta h] \end{cases} \tag{16}$$

where $[X_{\min}, X_{\max}]$ and $[Y_{\min}, Y_{\max}]$ are the x range and y range of the ROI, and Δw and Δh are its half width and height.

Once the ROI is determined, it is tracked in succeeding images.

B. Feature Lines Extraction

The stripe is thinned to its center line, which is computed based on the two borders of the laser stripe as follows:

$$C_l(j) = (E_u(j) + E_l(j))/2, \quad j \in [X_{\min}, X_{\max}] \tag{17}$$

$$E_u(j) = \arg\max_k G(k), k \in [Y_{\min}, Y_{\max}] \tag{18}$$

$$E_l(j) = \arg\min_k G(k), k \in [Y_{\min}, Y_{\max}] \tag{19}$$

where $C_l(j)$ is the center point on the laser stripe in jth column, $E_u(j)$ and $E_l(j)$ are the two points on the upper and lower borders.

Then, random sample consensus (RANSAC) algorithm is adopted to extract the two feature lines based on the thinned stripe earlier. RANSAC is an iterative method, which is robust to noise contained in the points. In the procedure of lines extraction, three conditions should be satisfied: 1) the difference between the intercepts of the two lines is bigger than a threshold; 2) since the welding is a slow process, the intercept change of each line in two subsequent sample time is less than a threshold; and 3) as long as the robot tracks the seam well, the difference between the feedback and reference image features is less than a threshold. The first condition is as follows:

$$|B_l(k) - B_r(k)| > B_{T1} \tag{20}$$

where $B_l(k)$ and $B_r(k)$ are the intercepts of the two lines at kth sample time, and B_{T1} is a threshold.

The second and third conditions for the left line are given in (21). The two conditions for the right line are similar to (21), which are omitted here

$$\begin{cases} |B_l(k) - B_l(k-1)| < B_{T2} \\ |B_{lf}(k) - B_{lr}(k)| < B_{T3} \end{cases} \tag{21}$$

where $B_{lf}(k)$ and $B_{lr}(k)$ are the feedback and reference intercepts of the left line, respectively, and B_{T2} and B_{T3} are two thresholds. After the two feature lines are obtained with RANSAC, least-square line fitting technique is employed in order to further improve the accuracy of the two lines. Since this process is the same for the two lines, here we take the left line for an example. Suppose the left line is as follows:

$$y = K_l x + B_l \tag{22}$$

where K_l and B_l are the slope and intercept of the left line, respectively.

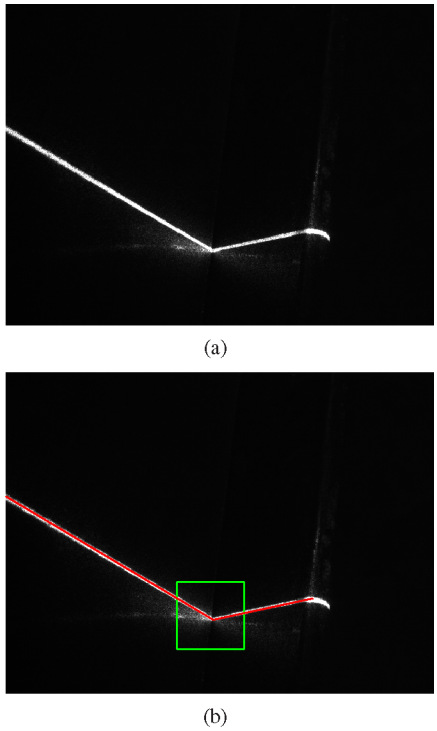

(a)

(b)

Fig. 5. Feature lines extraction. (a) Original image. (b) Extracted feature lines.

The parameters of the line after least-square fitting are as follows:

$$\begin{cases} K_l = \frac{(X-\bar{X})^T(Y-\bar{Y})}{(X-\bar{X})^T(X-\bar{X})} \\ B_l = \bar{y} - K_l \bar{x} \end{cases} \tag{23}$$

where $X = [x_1, x_2, \ldots, x_n]^T$, $Y = [y_1, y_2, \ldots, y_n]^T$, $\bar{X} = \bar{x}[1, 1, \ldots, 1]^T$, and $\bar{Y} = \bar{y}[1, 1, \ldots, 1]^T$. $(x_j, y_j)(j = 1, 2, \ldots, n)$ are the inner points, n is the their number, and $(\bar{x}, \bar{y})$ is the average coordinates of the inner points. The set of inner points I_p is defined as follows:

$$I_p = \{(x_j, y_j) | d_j < d_T\} \tag{24}$$

where d_T is the distance threshold, d_j is the distance of the point (x_j, y_j) from the line, which is computed by

$$d_j = \frac{|y_j - K_l x_j - B_l|}{\sqrt{1 + B_l^2}}. \tag{25}$$

To verify the effectiveness of the proposed feature-extraction method, a lot of images captured from the welding workshop were tested. The result of feature extraction for one image is shown in Fig. 5. Fig. 5(a) shows the original image. Fig. 5(b) shows the ROI of the seam image and the two extracted feature lines. It can be seen that the image features are favorably extracted using the proposed method.

IV. Proposed SFC

The proposed SFC is shown in Fig.6. It mainly consists of five parts: two independent fuzzy subcontrollers, a self-tuning mechanism, a supervisory level, and a vision sensor. The two

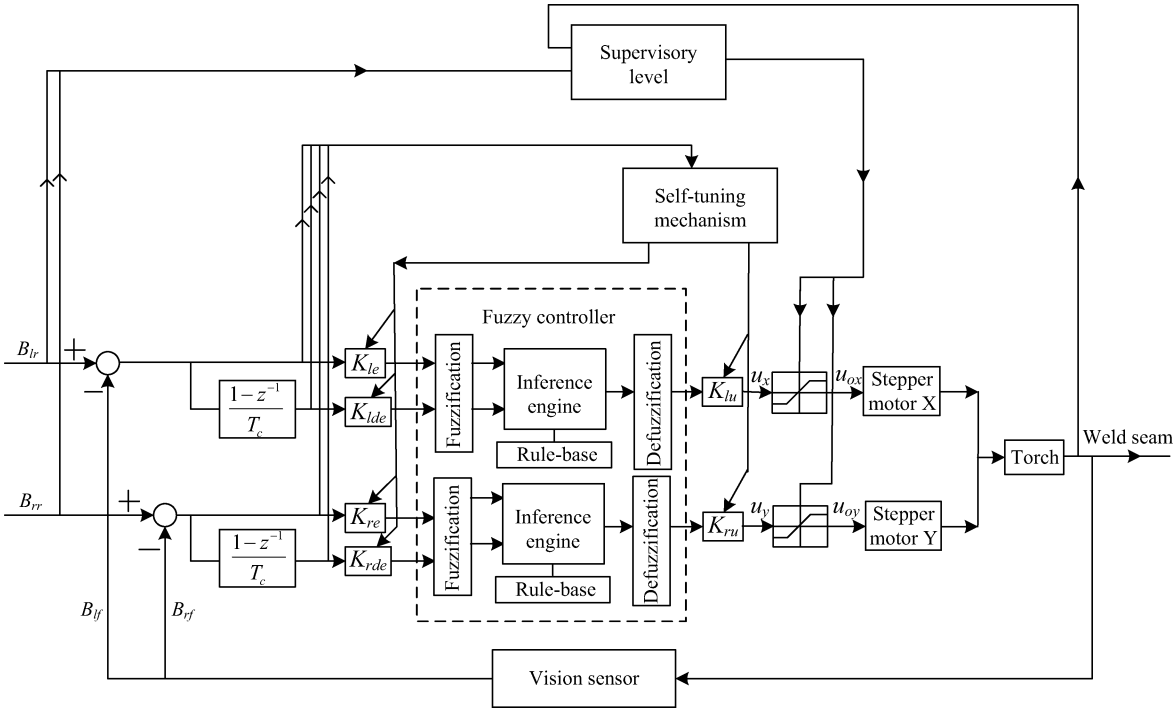

Fig. 6. Structure of the proposed SFC.

fuzzy subcontrollers are designed for the adjustment in the directions of the X_T-axis and Y_T-axis. As the RFC, each subcontroller contains three parts: fuzzification, inference engine, and defuzzification. Fuzzification maps the crisp inputs into fuzzy sets. Inference engine computes the fuzzy output based on the fuzzy input and rule base. The mostly used inference rule is the well-known Mamdani's Max–Min method, which is adopted in this paper. Defuzzification retransforms the fuzzy output into crisp one, which is used to control stepper motor. Three scaling factors are embedded in the input channels and output channels of the subcontrollers. They are used to transform the universes of discourse to suitable ones. The self-tuning mechanism is used to adjust the input and output scaling factors to improve the performance of the controller. The supervisory level is introduced into the controller hierarchy to keep steady and safe tracking. The reference and feedback image features are computed in the vision sensor. At the start stage in the welding process, the vision sensor outputs reference image feature. Then, the vision sensor gives feedback image feature.

The two fuzzy subcontrollers are designed similarly. As an example, the design of the one in X_T-axis direction is given as follows.

A. Membership Functions

The intercept B_{lr} is used as the reference and the intercept B_{lf} is served as the feedback. At sample instant k, the inputs to the fuzzy subcontroller are the error $e(k)$ and the differential error $de(k)$

$$e(k) = B_{lr}(k) - B_{lf}(k) \tag{26}$$

$$de(k) = e(k) - e(k-1) \tag{27}$$

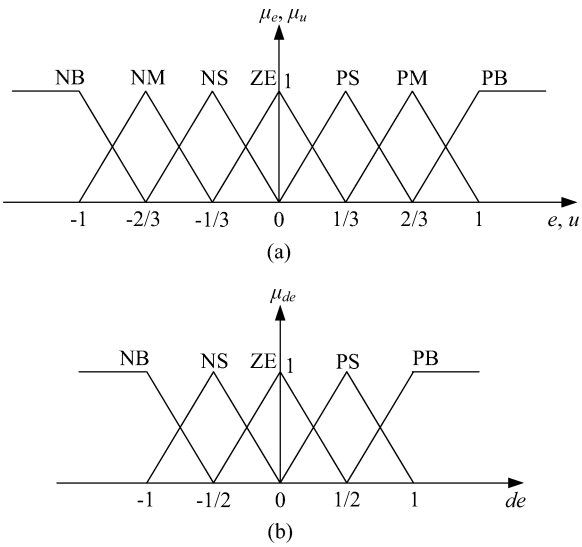

Fig. 7. Membership functions for e, de, and u.

where $B_{lr}(k)$ and $B_{lf}(k)$ are the reference and feedback image features, respectively.

Standard triangular membership functions with 50% overlap with neighboring membership functions are used for e, de, and the output u, as shown in Fig. 7. For e and u, the sets with seven linguistic values are defined, denoted as E and U. For de, the set with five linguistic values is defined, denoted as DE

$$E = \{\text{NB}, \text{NM}, \text{NS}, \text{ZE}, \text{PS}, \text{PM}, \text{PB}\} \tag{28}$$

$$DE = \{\text{NB}, \text{NS}, \text{ZE}, \text{PS}, \text{PB}\} \tag{29}$$

$$U = \{\text{NB}, \text{NM}, \text{NS}, \text{ZE}, \text{PS}, \text{PM}, \text{PB}\} \tag{30}$$

TABLE I
RULE BASE OF THE FUZZY CONTROLLER

U		E						
		NB	NM	NS	ZE	PS	PM	PB
DE	NB	NB	NB	NB	NM	NS	NS	ZE
	NS	NB	NB	NM	NS	NS	ZE	PS
	ZE	NB	NM	NS	ZE	PS	PM	PB
	PS	NS	ZE	PS	PS	PM	PB	PB
	PB	ZE	PS	PS	PM	PB	PB	PB

where NB, NM, NS, ZE, PS, PM, and PB are linguistic values meaning negative large, negative median, negative small, zero, positive small, positive median, and positive large, respectively.

Note that the universes of discourse for e, de, and u are all defined in $[-1, 1]$, which is achieved through the input and output scaling factors.

B. Rule Base

The rule base is the core of a fuzzy controller to specify the actions that should be taken under different conditions. It is the rule base that mostly represents the intelligence of the fuzzy controller. Each rule in the rule base has the IF–THEN form

$$\text{Rule i: if } e \text{ is } E_j \text{ and } de \text{ is } DE_k, \text{ then } u \text{ is } U_h \tag{31}$$

where E_j, DE_k, and U_h are the linguistic values in E, DE, and U, respectively.

Though the rule base can be obtained through training data, such as the one using decent training method [25], most are obtained from plant experts or through trial and error. In this paper, the rule base is designed from the authors' understanding of the seam-tracking system, as shown in Table I. To establish the rule base, two key factors are considered as follows.

1) When the error is large, the control action should quickly remove the error. For example, if e is NB and de is NB, then u is NB.
2) When the error is quickly reducing, the control action should avoid much overshoot. For example, if e is NB and de is PB, then u is ZE.

C. Defuzzification

Here, the commonly used center of gravity defuzzification method is adopted

$$u_c = \frac{\sum_{i=1}^{m} b_h \mu_i(E_j, DE_k, U_h, e, de)}{\sum_{i=1}^{m} \mu_i(E_j, DE_k, U_h, e, de)} \tag{32}$$

where u_c is the crisp output of the fuzzy controller, m is the number of rules in the rule base, b_h is the center of area of the membership function of the fuzzy set U_h in the consequent part of the given IF–THEN rule, and $\mu_i(E_j, DE_k, U_h, e, de)$ is the membership value of the ith rule, which is computed as follows:

$$\mu_i(E_j, DE_k, U_h, e, de) = \mu_{E_j}(e) \wedge \mu_{DE_k}(de) \wedge \mu_{U_h}(u). \tag{33}$$

D. Self-Tuning Mechanism

The input and output scaling factors are defined as follows:

$$K_e = \frac{2}{e_{\max} - e_{\min}} \tag{34}$$

$$K_{de} = \frac{2}{de_{\max} - de_{\min}} \tag{35}$$

$$K_u = \frac{u_{\max} - u_{\min}}{2} \tag{36}$$

where K_e, K_{de}, and K_u are the input and output scaling factors, $e_{\min}$, $de_{\min}$ and $u_{\min}$ are the lower limits of the crisp inputs and output of the fuzzy subcontroller, and $e_{\max}$, $de_{\max}$, and $u_{\max}$ are the corresponding upper limits.

As noted in the definition of the membership functions, the universes of discourse for inputs and output of the fuzzy subcontroller are all in the range of $[-1, 1]$, which is achieved by

$$e_s = K_e(e - e_{\min}) - 1 \tag{37}$$

$$de_s = K_{de}(de - de_{\min}) - 1 \tag{38}$$

$$u_s = K_u(u + 1) - u_{\min} \tag{39}$$

where e_s and de_s are the scaled inputs to the subcontroller, u_s is its scaled output, and u is its unscaled output.

For the RFC, the input and output scaling factors defined earlier are fixed in the whole welding process. Though the welding torch can track the seam when the scaling factors are fixed, the performance and tracking precision are not satisfactory. To improve the performance of the system, a self-tuning mechanism for the scaling factors is designed as follows.

$$SK_e = \beta_1 K_e = \frac{e_{\max} - e_{\min}}{e_{\max t} - e_{\min t}} K_e \tag{40}$$

$$SK_{de} = \beta_2 K_{de} = \frac{de_{\max} - de_{\min}}{de_{\max t} - de_{\min t}} K_{de} \tag{41}$$

$$SK_u = \beta_3 K_u = \beta_4 |e_{\max t} - e_{\min}| K_u \tag{42}$$

where SK_e, SK_{de}, and SK_u are the self-tuning scaling factors, β_1, β_2, and β_3 are the tuning coefficients, $e_{\min t}$, $de_{\min t}$, $e_{\max t}$, and $de_{\max t}$ are the lower and upper limits of the inputs of the subcontroller over time window T_w, and β_4 is a gain coefficient.

SK_e, SK_{de}, and SK_u are computed periodically. But the cycle to change these scaling factors, i.e., the time window T_w, should not be too short in order to have their steady values. The self-tuning mechanism is only activated when the error amplitude is bigger than a threshold, that is, $|e| > e_t$.

The input scaling factors determine the active region over which the fuzzy controller works. When the inputs to the controller are changed, the scaling factors are tuned to transform the working region to a new best one. Fig. 8 shows the effect of an input scaling factor on the active working region of the controller. When the input is small, the working region is confined to the region of ZE fuzzy set, which causes the controller to tune very slowly and the steady-state error to exist. In this case, the input scaling factor is adjusted to map the working region to the full range of the controller, resulting in improved input resolution. The range of the output of the controller needs to be

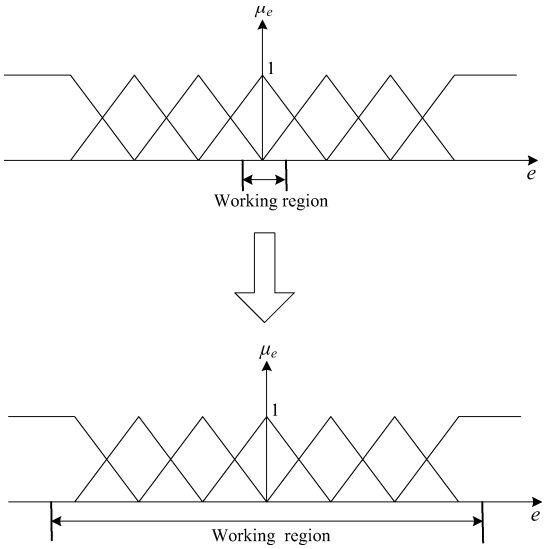

Fig. 8. Working region is changed by the input scaling factors.

changed according to the new input resolution, which is realized with the self-tuning output scaling factor. When the inputs of the controller are large, the output range of the controller should be large enough to quickly remove the errors. However, when the inputs of the controller are small, it should be kept small to avoid large oscillations around the set point.

E. Supervisory Level

The supervisory level is designed to limit the output pulses to a reasonable range, thus it can guarantee safety of the seam-tracking action. Since the offset of the workpiece from the tracks is not very large, the total output of the subcontroller in the whole welding process should be confined to a specific range. Moreover, the output pulses to the stepper motor at each step should be limited to keep steady tracking. Thus, as an example, the output to the stepper motor in the X_T-axis direction is as follows:

$$\begin{cases} u_o = u, & \text{if } |s_p| < s_l \text{ and } |u| < p_l \\ u_o = 0, & \text{if } |s_p| \geq s_l \\ u_o = -p_l, & \text{if } |s_p| < s_l \text{ and } u \leq -p_l \\ u_o = p_l, & \text{if } |s_p| < s_l \text{ and } u > p_l \end{cases} \tag{43}$$

where u_o is the output to the stepper motor in the X_T-axis direction, s_p is the total output, and p_l and s_l are the limited outputs to the stepper motor in one control period and the whole process, respectively.

V. Experiments and Results

To verify the effectiveness of the proposed tracking system and methods, a series of experiments were well conducted. The experimental system was shown in Fig. 9. The VC4018EC smart camera based on DSP and field-programmable gate array (FPGA) was used as the vision sensor and the OMRON PLC CP1H as the controller. The communication between the camera and the controller was based on series interface. The

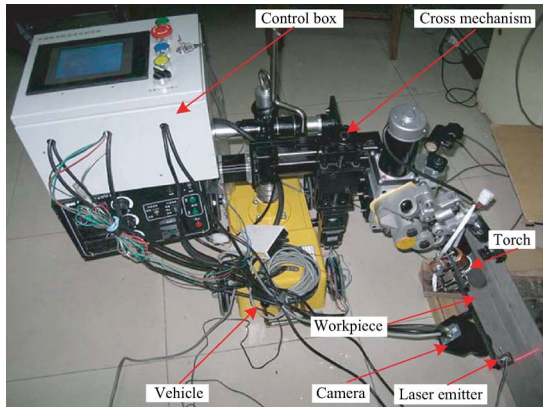

Fig. 9. Experimental system.

maximum frame rate of the camera was 30 frames per second, and its image size was 640 × 480 in pixel. The sample time of the system was 100 ms and all data was acquired at every sample time.

A. Seam-Tracking Result With the Proposed SFC

In the experiments, a fillet joint workpiece in about 1000 mm length was used. The torch was manually aligned with the welding seam before tracking. The workpiece was placed in such a way that the welding seam was not parallel to the tracks of the vehicle. The maximum offsets of the torch from the welding seam were 5.8 mm in X_T-axis direction and 9.6 mm in Y_T-axis direction, if the tracking was not active.

The parameters in the image processing were set as $\alpha_1 = 1$, $\alpha_2 = 2$, $\alpha_3 = 4$, $\alpha_4 = 2$, $\alpha_5 = 1$, $L = 7$, $K = 5$, $\Delta_w = \Delta_h = 50$ pixel, $B_{T1} = 50$, $B_{T2} = B_{T3} = 10$, and $d_T = 2$ pixel. The lower and upper limits of the inputs and outputs for the fuzzy subcontrollers were given as $e_{\max} = 10$, $e_{\min} = -10$, $de_{\max} = 5$, $de_{\min} = -5$, $u_{\max} = 100$, and $u_{\min} = -100$. The time window T_w for adjusting the scaling factors was set 1 s. The gain coefficient β_4 was 0.8. The threshold e_t was set 1 pixel. The limited outputs to the stepper motor for one control period and the whole process were set to $p_l = 200$ pulses and $s_l = 3000$ pulses. The tracking results in one experiment are shown in Figs. 10–12. Fig. 10 shows the image errors and the tuning of scaling factors of the corresponding SFC. It can be seen that the torch tracked the welding seam satisfactorily. The largest image error of the intercept of the left line was 2 pixels and that of the right line was 3 pixels. The scale factor from Cartesian space to image space calibrated in practice was 0.06 mm/pixel. Thus, the largest tracking error in Cartesian space in X_T-axis direction was 0.12 mm and in Y_T-axis direction 0.18 mm. Fig. 11 shows the reference and tracked torch trajectories in the tracking process. The torch position was measured in the world frame W, which was established in the initial welding position when torch was manually aligned with the seam. Its X_W-axis and Y_W-axis were parallel with X_T-axis and Y_T-axis of the tool frame T. The trajectory of the torch shows that the torch followed the seam well. The weld shape of the fillet joint after welding with the SFC is shown in Fig. 12. It demonstrates

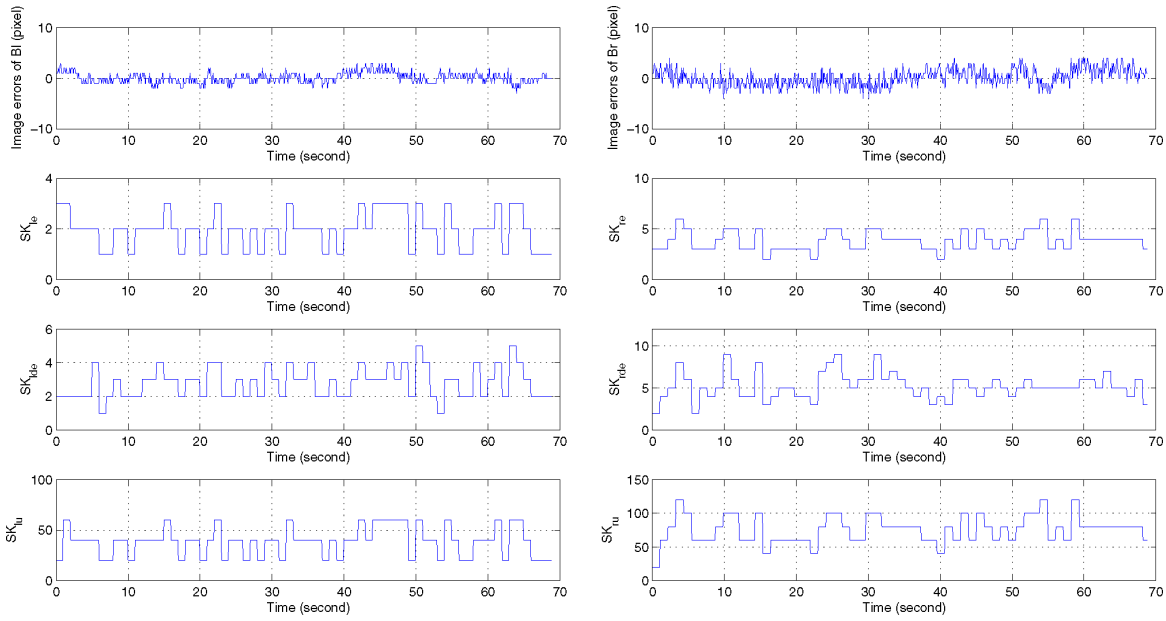

Fig. 10. Image errors and the tuning of input and output scaling factors of two SFC's. (a) Left intercept and the scaling factors of the corresponding SFC. (b) Right intercept and the scaling factors of the corresponding SFC.

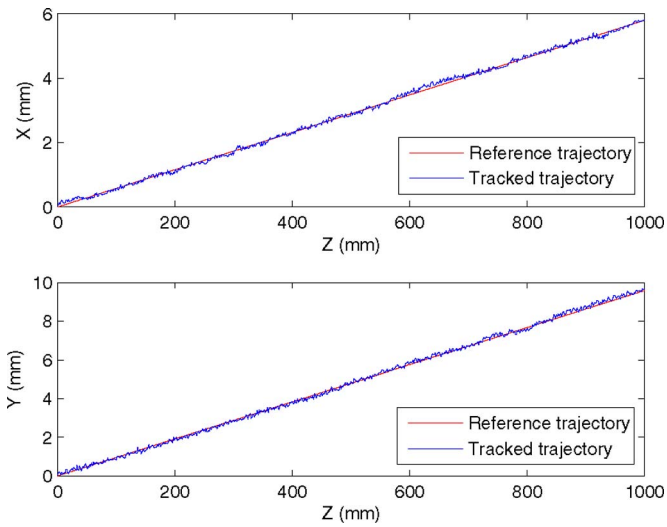

Fig. 11. Reference and tracked trajectories of the torch with the SFC.

Fig. 12. Weld shape of fillet joint after welding with the SFC.

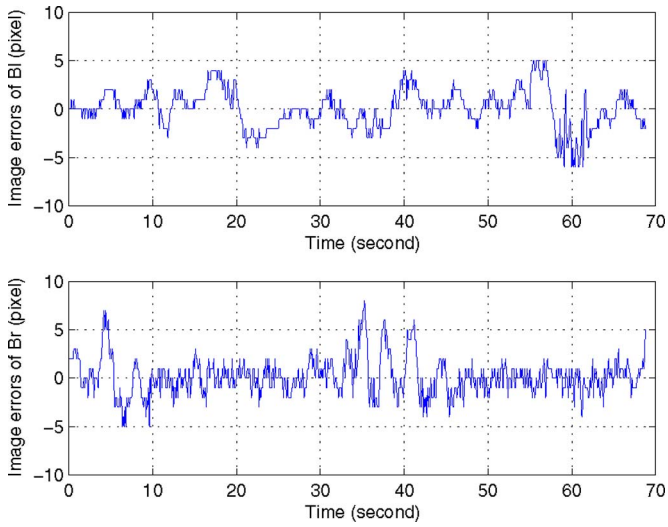

Fig. 13. Image errors of the intercepts of the laser stripe with the RFC.

that good weld shape can be achieved using this seam-tracking system.

B. Seam-Tracking Result With RFC

Comparison experiments were conducted using RFC. The parameters set for RFC were the same as SFC except those used in the self-tuning mechanism. The input and output scaling factors for the two RFC's were the same. They were fixed in the tracking process, which were set as: $K_e = 10$, $K_{de} = 5$, and $K_u = 100$. The experimental results with RFC are shown in Figs. 13 and 14. Fig. 13 shows the image errors of the intercepts of the two stripe lines, and Fig. 14 shows the reference and tracked torch trajectories. Compared with the tracking results

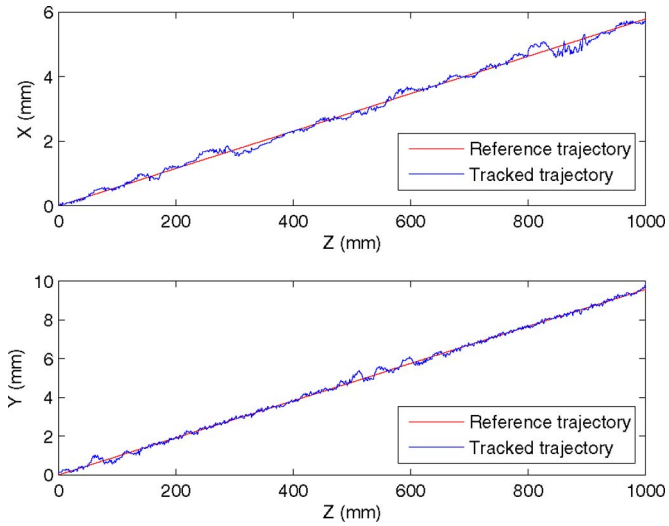

Fig. 14. Reference and tracked trajectories of the torch with the RFC.

TABLE II
COMPARISON OF SEAM-TRACKING PERFORMANCE BY RFC AND THE PROPOSED SFC

Controller	MHE (mm)	MVE (mm)	LHE (mm)	LVE (mm)
SFC	0.04	0.07	0.12	0.18
RFC	0.09	0.11	0.36	0.48

MHE: Mean horizontal error, MVE: mean vertical error, LHE: largest horizontal error, and LVE: largest vertical error.

with the proposed SFC, it can be seen that the image errors with RFC were bigger and more oscillations occurred in the torch trajectory. For better illustration, the test results were compared in Table II. The mean errors were computed based on 680 sample data that were gathered in the real-time seam tracking. From Table II, it can be seen that the mean errors were almost doubled with RFC and the largest errors were almost tripled. Thus, it is obvious that the proposed SFC outperforms the RFC.

C. Comparison Experiment With the Proposed SFC and PID Controller to a Large Step Disturbance

To validate the proposed controller further, comparison experiments were conducted with the proposed SFC and conventional PID controller. The parameters for PID controllers in two directions were tuned beforehand with Ziegler–Nichols method. The proportional, integral, and derivative gains of the PID controller in X_T-axis direction were 0.8, 0.16, and 0.02 and those in Y_T-axis were 0.2, 0.08, and 0.002. The parameters for the SFC were the same as the experiments in Section V-A. In the tracking process, the workpiece was quickly moved about 10 mm in the Y_T-axis direction to manually form a step offset as a large disturbance. The tracking errors for the SFC's and PID controllers in one experiment are given in Fig. 15. It can be found that the SFC in Y_T-axis direction could recover the tracking from the disturbance in about 6 s, and then, the

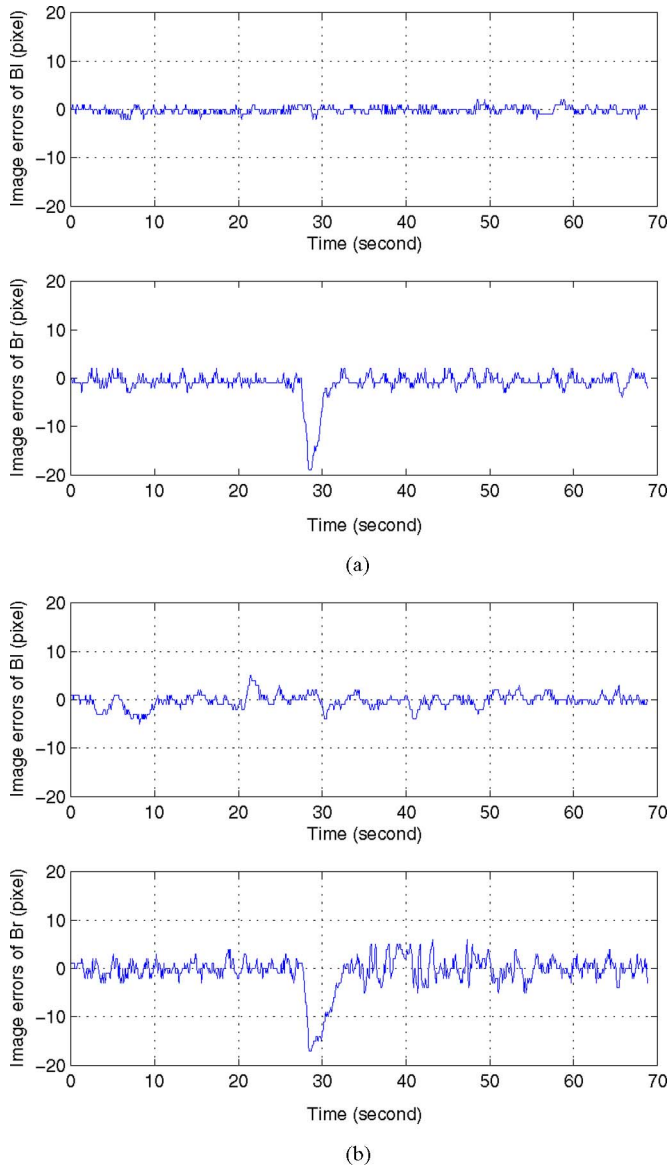

Fig. 15. Comparison tracking results with two controllers to a large step disturbance. (a) Image errors with the proposed SFC. (b) Image errors with PID controller.

tracking accuracy was kept. The PID controller in Y_T-axis direction needed about 10 s to recover, and then, the tracking accuracy reduced. Moreover, the tracking accuracy of the SFC in X_T-axis direction outperformed the one of the PID controller. From the comparison experiments, it can be seen that the proposed SFC is more robust. Its response is more steady and the tracking accuracy is higher.

VI. CONCLUSION

A fillet weld seam-tracking system with vision feedback was designed in this paper. The image features were properly selected to get an almost uncoupled and linear control model. A two-step feature-extraction method was proposed to robustly detect the two lines of the laser stripe. In order to improve the tracking performance, a new SFC was designed. The self-tuning

mechanism of the fuzzy controller is based on the principle that its active working region is determined by the input scaling factors. Moreover, a supervisory level is added to the controller hierarchy to guarantee the safety and steadiness of the tracking action.

The experimental results show that the proposed seam-tracking system can track the fillet joint satisfactorily. From the comparison experiments, it can be seen that the tracking accuracy of the proposed SFC is better than that of RFC, and that the proposed SFC is more robust to disturbances than conventional PID controller.

Only a fillet weld joint is considered in this paper, but the proposed SFC can be extended to other joint types, such as butt joint, lap joint, V-groove joint, etc., with the selections of corresponding image features. In addition, camera's affine projection model is used in this paper, which is a linear approximation to the pinhole model. When higher tracking accuracy is required, the camera's pinhole model should be used. With the pinhole model, the slopes of the two stripe lines will be slightly changed in the tracking process and the adjustments in two directions will have coupling. This problem can be handled by adding some elaborate regulation rules to the fuzzy controllers.

REFERENCES

[1] C. I. Umeagukwu, B. Maqueira, and R. Lambert, "Robotic acoustic seam tracking: System development and application," *IEEE Trans. Ind. Electron.*, vol. 36, no. 3, pp. 338–348, Aug. 1989.

[2] F. A. H. M. Jäger and S. Humbert, "Sputter tracking for the automatic monitoring of industrial laser-welding processes," *IEEE Trans. Ind. Electron.*, vol. 55, no. 5, pp. 2177–2184, May 2008.

[3] Z. Bingul, G. E. Cook, and A. M. Strauss, "Application of fuzzy control to spatial thermal control in fusion welding," *IEEE Trans. Ind. Appl.*, vol. 36, no. 6, pp. 1523–1530, Nov./Dec. 2000.

[4] J. W. Kim and J. H. Shin, "A study of a dual-electromagnetic sensor system for weld seam tracking of I -butt joints," in *Proc. Instn. Mech. Engrs., J. Eng. Manuf.*, 2003, vol. 217, pp. 1305–1313.

[5] K. Y. Bae and J. H. Park, "A study on development of inductive sensor for automatic weld seam tracking," *J. Mater. Proc. Technol.*, vol. 176, pp. 111–116, 2006.

[6] H. Fennander, V. Kyrki, A. Fellman, A. Salminen, and H. Kalviainen, "Visual measurement and tracking in laser hybrid welding," *Mach. Vis. Appl.*, vol. 20, pp. 103–118, 2009.

[7] E. C. Dean, V. P. Vega, and A. E. Romero, "Visual servoing for constrained planar robots subject to complex friction," *IEEE/ASME Trans. Mechatronics*, vol. 11, no. 4, pp. 389–400, Aug. 2006.

[8] M. Bonkovic, A. Hace, and K. Jezernik, "Population-based uncalibrated visual servoing," *IEEE/ASME Trans. Mechatronics*, vol. 13, no. 3, pp. 393–397, Jun. 2008.

[9] Y. T. Shen, D. Sun, Y. H. Liu, and K. J. Li, "Asymptotic trajectory tracking of manipulators using uncalibrated visual feedback," *IEEE/ASME Trans. Mechatronics*, vol. 8, no. 1, pp. 87–98, Mar. 2003.

[10] C. L. Hwang and L. J. Chang, "Trajectory tracking and obstacle avoidance of car-like mobile robots in an intelligent space using mixed h_2/h_∞ decentralized control," *IEEE/ASME Trans. Mechatronics*, vol. 12, no. 3, pp. 345–352, Jun. 2007.

[11] D. Xu, L. K. Wang, Z. G. Tu, and M. Tan, "Hybrid visual servoing control for robotic arc welding based on structured lignt vision," *Acta Automatica Sinica*, vol. 31, pp. 596–605, 2005.

[12] M. Y. Kim, K. W. Ko, H. S. Cho, and J. H. Kim, "Visual sensing and recognition of welding environment for intelligent shipyard welding robots," in *Proc. IEEE Int. Conf. Intell. Robot. Syst*, Takamatsu, Japan, Nov. 2000, pp. 2159–2165.

[13] S. K. Lee and S. J. Na, "A study on automatic seam tracking in pulsed laser edge welding by using a vision sensor without an auxiliary light source," *J. Manuf. Syst.*, vol. 21, pp. 302–315, 2002.

[14] S. Hutchinson, G. D. Hager, and P. I. Corke, "A tutorial on visual servo control," *IEEE Trans. Robot. Autom.*, vol. 12, no. 5, pp. 651–670, Oct. 1996.

[15] P. Sicard and M. D. Levine, "Joint recognition and tracking for robotic arc welding," *IEEE Trans. Syst., Man, Cybern.*, vol. 19, no. 4, pp. 714–728, Jul./Aug. 1989.

[16] J. S. Kim, Y. T. Son, H. S. Cho, and K. Koh, "A robust method for vision-based seam tracking in robotic arc welding," in *Proc. IEEE Int. Symp. Intell. Contr.*, Monterey, CA, Aug. 1995, pp. 363–368.

[17] Z. Bingul and G. E. Cook, "A real-time prediction model of electrode extension for GMAW," *IEEE/ASME Trans. Mechatronics*, vol. 11, no. 1, pp. 47–54, Feb. 2006.

[18] R. E. Precup, S. Preitl, I. J. Rudas, M. L. Tomescu, and J. K. Tar, "Design and experiments for a class of fuzzy controlled servo systems," *IEEE/ASME Trans. Mechatronics*, vol. 13, no. 1, pp. 22–35, Feb. 2008.

[19] L. Yao and P. Z. Huang, "Learning of hybrid fuzzy controller for the optical data storage device," *IEEE/ASME Trans. Mechatronics*, vol. 13, no. 1, pp. 3–13, Feb. 2008.

[20] M. Cheng, Q. Sun, and E. Zhou, "New self-tuning fuzzy PI control of a novel doubly salient permanent-magnet motor drive," *IEEE Trans. Ind. Electron.*, vol. 53, no. 3, pp. 814–821, Jun. 2006.

[21] F. C. Teng, A. Lotfi, and A. C. Tsoi, "Self-tuning PD+I fuzzy logic controller with minumum number of rules," in *Proc. IEEE Int. Conf. Syst. Man. Cybern.*, Polytech. Univ. of Puerto Rico, San Juan, Oct. 2007, pp. 865–870.

[22] W. A. Kwong and K. M. Passino, "Dynamically focused fuzzy learning control," *IEEE Trans. Syst., Man, Cybern. B*, vol. 26, no. 1, pp. 53–74, Jan. 1996.

[23] G. Langari and M. Tomizuka, "Self organizing fuzzy linguistic control with application to arc welding," in *Proc. IEEE Int. Workshop Intell. Robot. Syst.*, Ibaraki, Japan, Jul.1990, pp. 1007–1014.

[24] J. R. Layne and K. M. Passino, "Fuzzy model reference learning control," *J. Intell. Fuzzy. Syst.*, vol. 4, pp. 33–47, 1996.

[25] H. Nomura, I. Hayashi, and N. Wakami, "A learning method of fuzzy inference rules by descent method," in *Proc. IEEE Int. Fuzzy Syst. Conf.*, San Diego, CA, Mar. 1992, pp. 203–210.

Zaojun Fang received the B.Sc. degree from the University of Science and Technology Liaoning, Anshan, China, in 2005, and the M.Sc. degree from the Institute of Automation, Chinese Academy of Sciences (IACAS), Beijing, China, in 2008, both in control science and engineering. He is currently working toward the Ph.D. degree at IACAS.

His current research interests include robotics and automation.

De Xu (M'05–SM'10) received the B.Sc. and M.Sc. degrees from Shandong University of Technology, Jinan, China, in 1985 and 1990, respectively, and the Ph.D. degree from Zhejiang University, Hangzhou, China, in 2001, all in control science and engineering.

Since 2001, he has been with the Institute of Automation, Chinese Academy of Sciences (IACAS), Beijing, China, where he is currently a Professor in the Laboratory of Complex Systems and Intelligence Science. His research interests include robotics and automation, in particular, the control of robots, such as visual control and intelligent control.

Min Tan received the B.Sc. degree from Tsing Hua University, Beijing, China, in 1986, and the Ph.D. degree from the Institute of Automation, Chinese Academy of Sciences (IACAS), Beijing, in 1990, both in control science and engineering.

He is currently a Professor in the Laboratory of Complex Systems and Intelligence Science, IACAS. He has authored or coauthored more than 100 papers in journals, books, and conference proceedings. His research interests include robotics and intelligent control systems.

View publication stats